Development of a Medium Voltage, High Power, High Frequency Four-Port Solid State Transformer

Ahmad El Shafei, *Member, IEEE*, Saban Ozdemir, *Senior Member, IEEE*, Necmi Altin, *Senior Member, IEEE*, Garry Jean-Pierre, *Member, IEEE*, and Adel Nasiri, *Fellow, IEEE*

***Abstract*—The power and voltage levels of renewable energy resources is growing with the evolution of the power electronics and switching module technologies. For that, the need for the development of a compact and highly efficient solid-state transformer is becoming a critical task in-order to integrate the current AC grid with the new renewable energy systems. The objective of this paper is to present the design, implementation, and testing of a compact multi-port solid-state transformer for microgrid integration applications. The proposed system has a four-port transformer and four converters connected to the ports. The transformer has four windings integrated on a single common core. Thus, it can integrate different renewable energy resources and energy storage systems. Each port has a rated power of 25kW, and the switching frequency is pushed to 50kHz. The ports are chosen to represent a realistic industrial microgrid model consisting of grid, energy storage system, photovoltaic system, and load. The grid port is designed to operate at 4.16kVAC corresponding to 7.2kV DC bus voltage, while the other three ports operate at 500VDC. Moreover, the grid, energy storage and photovoltaic ports are active ports with dual active bridge topologies, while the load port is a passive port with full bridge rectifier one. The proposed design is first validated with simulation results, and then the proposed transformer is implemented and tested. Experimental results show that the designed system is suitable for 4.16kVAC medium voltage grid integration.**

***Index Terms*— Co-simulation, high frequency, high power, medium voltage, microgrid, Multi-port, solid state transformer.**

I. Introduction

THE concept of Solid-State Transformer (SST) utilizes a high/medium frequency transformer applied in a power electronic converter. An increase in the operating frequency will make the volume and power density level superior to the traditional 50/60Hz transformers. Modern advancements in the magnetic material discoveries as well as high frequency switching modules development made it possible to have the desirable highly efficient high-power density SSTs. The new technologies allow the system to have a high saturation flux density, low core power loss, and low switching & conducting losses [1]-[3]. Many studies have been projected lately on SST design and applications [4]-[11]. However, most of these studies are based on conventional two-ports transformers. The significant increase in the number of Distributed Generations (DGs) and the significance of microgrid concepts has shaped the need for a single compact element integrating multiple renewable sources. This triggered the idea of a Multi-Port Solid State Transformer (MPSST) concept. Few articles and research work have been directed towards this concept [12]-[19]. To get rid of using several power electronic converters which utilize only two windings solid state transformers, a multi-port solid state transformer can reduce the overall system volume and increase its efficiency and power density.

Although MPSST has multiple ports, it is still a kind of modified Dual Active Bridge (DAB) topology. As it is well known, leakage inductance is one of the most important parameters in these converters. A small leakage inductor value increases the di/dt ratio on the switch current and forces the switch to its limitation. In addition, for the same power level, current crest factor will increase, and it will result in an increase in system losses [20]. On the other hand, the high value of leakage inductance raises other problems especially if an external inductor is utilized in the system topology. The maximum amount of power that can be transferred to the secondary side of the DAB converter is directly related to the leakage inductance. A high leakage inductance value limits the power throughput transfer capability.

The leakage inductance value depends basically on the winding placement, core geometry, insulation thickness, and hence, coupling coefficient between the windings. In addition, system requirements such as power density, high efficiency, medium voltage insulation specification, partial discharge, etc. will increase the complexity of the transformer design. For a multi-port transformer system, design of the high frequency transformer and achieving the needed leakage inductance value is even more difficult [6]. Incorporation of several renewable energy resources in a single compact system will be a major design breakthrough for the upcoming smart distribution systems.

Manuscript received September 11, 2020; revised December 31, 2020; accepted August 10, 2021. date of publication March 25, 2022; date of current version March 18, 2022.

This material is based upon work supported by the National Science Foundation under Grant No. 1650470, GRAPES I/UCRC program.

A. El Shafei is with Department of Electrical Engineering, University of Wisconsin Milwaukee, Milwaukee, WI 53212 USA (e-mail: aie@uwm.edu).

S. Ozdemir and N. Altin are with Department of Electrical-Electronic Engineering, Faculty of Technology, University of Gazi, 06500 Ankara, Turkey (e-mail: sabanozdemir@gazi.edu.tr, naltin@gazi.edu.tr).

G. Jean-Pierre was with Department of Electrical Engineering, University of Wisconsin Milwaukee, Milwaukee, WI 53212, USA (e-mail: jeanpie4@uwm.edu)

A. Nasiri was with Department of Electrical Engineering, University of Wisconsin Milwaukee, Milwaukee, WI 53212 USA. Now he is with Department of Electrical Engineering, University of South Carolina, Columbia, SC, 29208 USA (e-mail: nasiri@mailbox.sc.edu)

(Corresponding Author: Adel Nasiri)

Digital Object Identifier 10.30941/CESTEMS.2022.00013

In this paper, integration of four different ports will be discussed and presented. The four-port SST could be exploited in micro and smart grid applications. This research work aims at a rated power of 25kW for each connected port. The different ports can exemplify different DGs such as photovoltaic system, energy storage, and wind turbine. In this research paper, the first port illustrates a 4.16kVAC utility grid, while the other three ports operate at 500VDC representing an energy storage, photovoltaic, and a regulated passive load system. The goal is to demonstrate the operation and functionality of the medium voltage multi-port solid state transformer theory, thus, it will be assumed that a 7.4kV DC bus (corresponding to 4.16kVAC) and three 500V DC buses (corresponding to the energy storage, PV, and load) are available. The passive load port will be connected to a full bridge rectifier, while the other three active ports will be connective to DAB converters operating at 50kHz switching frequency. Furthermore, the energy storage and utility grid ports will be considered as bi-directional ports so that power can either be delivered or absorbed, while the PV will be unidirectional one. Fig. 1 summarizes the four-port SST system that will be studied in this paper.

There are two major challenges in this system: power flow control between the four ports as well as designing, building, and testing of the four-windings 50kHz medium voltage SST. In this paper, the focus is being directed towards the latter point, while the control study has been developed and published in [21]. Transformer modeling complexity incorporates several tradeoffs that should be carefully studied and adjusted for. A detailed analysis has been performed in-order to examine the desired transformer core material/shape/size/volume, windings placement/configuration/ number of turns, insulation level, leakage/magnetizing inductances, transformer core & copper losses, efficiency, and power density. The design and modeling have been carried throughout a Finite Element Analysis (FEA) simulation. The SST model functionality is verified by ANSYS Maxwell-3D and ANSYS Simplorer co-simulation studies. Then, the designed transformer and converter are implemented and tested for results validation and proof of the medium voltage multi-port solid state transformer (MV MPSST) concept. Experimental results will be shown at the end of this work.

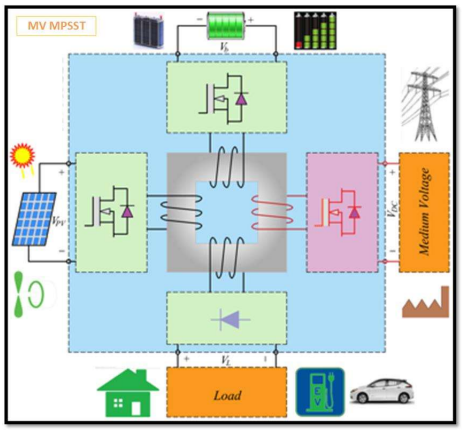

Fig. 1: Four-ports medium voltage solid state transformer (MV MPSST)

II. Transformer Design Procedure

In high frequency transformer design, several tasks & studies must be conducted in parallel. For instance, determination of mechanical parameters and material selection is considered a critical design issue. Defining these parameters directly affects the electrical parameters such as leakage inductance, energy density, and efficiency.

TABLE I.
Core Material Comparison

Material	Flux Density	1/Price	Frequ-ency	Dimension Avaliability	1/Loss
Ferrite	*	***	****	***	****
Amorphous	***	**	**	**	**
Silicon Steel	****	****	*	****	*
Nanocrysta-lline	**	*	***	**	***

A. Core Selection

The commonly used transformer core materials are si-steel, ferrite, nanocrystalline, and amorphous. The MV MPSST transformer must use the optimal material for the 50kHz, 25kW/port application. A literature review has been performed to compare the material characteristics at the systems' rated voltages, power, and switching frequency levels. A summary of the properties of the core materials is given in Table I. Analyzing the material differences sorted out silicon steel and amorphous and focused on ferrite and nanocrystalline cores. Although the flux density of the nanocrystalline are high compared to ferrite core, nanocrystalline loses its advantages over ferrite when the frequency increases in terms of core loss. In addition, the ferrite core is an easily available material in terms of size, shape, and commercial availability. Consequently, ferrite 3C94 material has been used for the MV MPSST transformer.

Shape of the transformer is critical as it affects the leakage inductance value, core cross-sectional area, volume, energy density, and thus, the transformer overall size and compactness. Designing a challenging system as the MV MPSST has two critical constraints to be studied and accommodated for: avoiding the core saturation and minimizing the leakage inductance. The core-shape and shell-type configurations have been studied on a 330kW 50kHz two-port transformer [4]. Compared results between the two shapes proved that the shell-type configuration increases the transformer efficiency and has lower leakage inductance than the core-type one. Subsequently, the shell-type has been chosen as the MV MPSST core configuration. Therefore, the three low voltage windings will be interleaved in the middle leg to maximize the coupling coefficient, and the medium voltage winding will be placed on top of them taking into consideration careful insulation.

B. Transfomer Formulation

Mathematical formulations for transformer characterization and operation have been derived. A MATLAB optimization algorithm has been developed in-order to choose the transformer parameters as a starting point for the modeling phase. Some equations used in the design optimization phase are given below. The relation between the product of mechanical dimensions with power rating, current density, flux density and frequency is given in Eq (1):

$$A_P = A_C W_a = \frac{S}{K_f K_{cu} B_m f J} 10^4 \quad (1)$$

where J is the current density, f is the switching frequency, B_m is the maximum flux density, A_c is the core cross-sectional area, A_p is the product area, W_a is the window area, S is the rated power, K_f is the waveform coefficient, and K_{cu} is the window utilization factor.

Transformer equations for induced voltage, core loss, winding loss, maximum flux density and number of turns are summarized below:

$$v(t) = N\frac{d\phi(t)}{dt} = NA_C\frac{dB(t)}{dt}v(t) \quad (2)$$

$$P_{Core} = k_{ref} B^{\beta} f^{\alpha} \quad (3)$$

$$B_m = \frac{V}{4xfxNxA_C} \quad (4)$$

$$N = \frac{V}{K_f A_C B_m f}\left(1 - \frac{T_d}{\pi}\right) \quad (5)$$

where V denotes the induced voltage, N number of turns, I rated current, P_{core} core losses, k_{ref}, β and α core coefficients extracted from the material datasheet, α wire coefficient, P_{sw} switching losses, and T_d dead-time for switches.

C. Four-port Transformer Equivalent Circuit Derivation

In this section, a systematic approach for calculating the leakage and magnetizing inductances and obtaining the equivalent circuit of MPSST is presented. This method generates a model for the given MPSST structure. Then, the four-port MPSST inductance matrix which includes the self and mutual inductances is extracted from ANSYS Maxwell-3D simulation for this model. Finally, the leakage and magnetizing inductances which define the equivalent circuit of the MPSST are calculated by using derived mathematical equations and this inductance matrix.

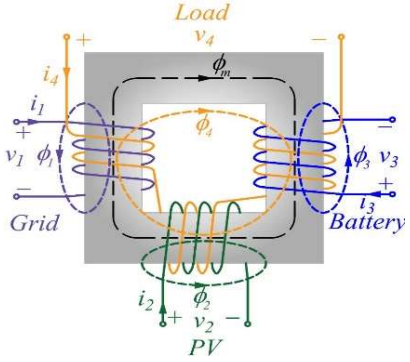

Fig. 2. General MPSST Configuration.

As seen from Fig. 2 for a general MPSST configuration, all ports are magnetically coupled and form self and mutual fluxes which have effects on power transfer among the interacting ports. The analysis process is as summarized in the flowchart given in Fig. 3.

As a first step, fluxes equations are written, and induced voltage equations are derived by using Faraday's law [22], [23]:

$$v_1 = N_1 \cdot \frac{d}{dt}\left[\phi_m + \phi_1 + \phi_{1-2} + \phi_{1-3} + \phi_{1-4} + \phi_{1-2-3} + \phi_{1-2-4} + \phi_{1-3-4}\right] \quad (6)$$

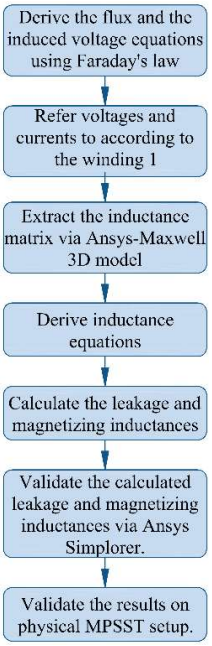

Fig. 3. Flowchart of the MPSST analysis process.

$$v_2 = N_2 \cdot \frac{d}{dt}\left[\phi_m + \phi_2 + \phi_{1-2} + \phi_{2-3} + \phi_{2-4} + \phi_{1-2-3} + \phi_{2-3-4} + \phi_{1-2-4}\right] \quad (7)$$

$$v_3 = N_3 \cdot \frac{d}{dt}\left[\phi_m + \phi_3 + \phi_{1-3} + \phi_{2-3} + \phi_{3-4} + \phi_{1-2-3} + \phi_{2-3-4} + \phi_{1-3-4}\right] \quad (8)$$

$$v_4 = N_4 \cdot \frac{d}{dt}\left[\phi_m + \phi_4 + \phi_{1-4} + \phi_{2-4} + \phi_{3-4} + \phi_{2-3-4} + \phi_{1-2-4} + \phi_{1-3-4}\right] \quad (9)$$

where N_i is the number of turns of winding i (for i=1,2,3,4); ϕ_m is the main flux linking all four windings, ϕ_i is the self-leakage flux, and ϕ_{i-j} and ϕ_{i-j-k} are the mutual fluxes. The flux equations can be written as:

$$\phi_m = P_m \cdot \left(N_1 \cdot i_1 + N_2 \cdot i_2 + N_3 \cdot i_3 + N_4 \cdot i_4\right) \quad (10)$$

$$\phi_i = P_i \cdot \left(N_i \cdot i_i\right) \text{ for } i=1,2,3,4 \quad (11)$$

$$\phi_{i-j} = P_{i-j} \cdot \left(N_i \cdot i_i + N_j \cdot i_j\right),\ i=1,2,3\ \ j=2,3,4 \text{ and } i \neq j \quad (12)$$

$$\phi_{i-j-k} = P_{i-j-k} \cdot \left(N_i \cdot i_i + N_j \cdot i_j + N_k \cdot i_k\right), \text{ for } i=1,2 \text{ and } j=2,3 \text{ and } k=3,4 \text{ and } i \neq j \neq k \quad (13)$$

Here, P_m is the permeance across the main magnetic path ϕ_m; P_i is the permeance across magnetic path ϕ_i; P_{i-j} s the permeance across magnetic path ϕ_{i-j} (for i=1,2,3 and j=2,3,4 and $i \neq j$), and P_{i-j-k} is the permeance across magnetic path ϕ_{i-j-k} (for i=1,2 and j=2,3 and k=3,4 and $i \neq j \neq k$).

If flux equations are substituted and re-arrangements are done, the voltage equation is obtained as:

$$\begin{aligned} v_1 = {} & N_1^2 \cdot \frac{di_1}{dt}\left(P_m + P_1 + P_{1-2} + P_{1-3} + P_{1-4} + P_{1-2-3} + \right. \\ & \left. P_{1-2-4} + P_{1-3-4}\right) + N_1 . N_2 \cdot \frac{di_2}{dt} \cdot \left(P_m + P_{1-2} + P_{1-2-3} + P_{1-2-4}\right) + \\ & N_1 . N_3 \cdot \frac{di_3}{dt} \cdot \left(P_m + P_{1-3} + P_{1-2-3} + P_{1-3-4}\right) + \\ & N_1 . N_4 \cdot \frac{di_4}{dt} \cdot \left(P_m + P_{1-4} + P_{1-2-4} + P_{1-3-4}\right) \end{aligned} \quad (14)$$

Similarly, v_2, v_3, and v_4 are derived and formulated. The ports voltages and currents can be referred to the first winding by using:

$$v_i = \frac{N_i}{N_1}\cdot v_{i-1} \text{ and } i_i = \frac{N_1}{N_i}\cdot i_{i-1} \tag{15}$$

where v_{i-1} , i_{i-1} are voltage and current of the *i-th* winding reflected to the first winding, respectively. Then, the reflected ports voltages can be written as:

$$\begin{aligned} v_1 &= N_1^2.\frac{di_1}{dt}\left(P_m + P_1 + P_{1-2} + P_{1-3} + P_{1-4} + P_{1-2-3} + P_{1-2-4} + P_{1-3-4}\right) + \\ &N_1^2.\frac{di_{2-1}}{dt}.\left(P_m + P_{1-2} + P_{1-2-3} + P_{1-2-4}\right) + \\ &+N_1^2.\frac{di_{3-1}}{dt}.\left(P_m + P_{1-3} + P_{1-2-3} + P_{1-3-4}\right) + \\ &N_1^2.\frac{di_{4-1}}{dt}.\left(P_m + P_{1-4} + P_{1-2-4} + P_{1-3-4}\right) \end{aligned} \tag{16}$$

$$\begin{aligned} v_{2-1} &= N_1^2.\frac{di_1}{dt}\left(P_m + P_{1-2} + P_{1-2-3} + P_{1-2-4}\right) + \\ &N_1^2.\frac{di_{2-1}}{dt}.\left(P_m + P_2 + P_{1-2} + P_{2-3} + P_{2-4} + P_{1-2-3} + \right. \\ &\left. P_{2-3-4} + P_{1-2-4}\right) + N_1^2.\frac{di_{3-1}}{dt}.\left(P_m + P_{2-3} + P_{1-2-3} + \right. \\ &\left. P_{2-3-4}\right) + N_1^2.\frac{di_{4-1}}{dt}.\left(P_m + P_{2-4} + P_{2-3-4} + P_{1-2-4}\right) \end{aligned} \tag{17}$$

$$\begin{aligned} v_{3-1} &= N_1^2.\frac{di_1}{dt}\left(P_m + P_{1-3} + P_{1-2-3} + P_{1-3-4}\right) + \\ &N_1^2.\frac{di_{2-1}}{dt}.\left(P_m + P_{2-3} + P_{1-2-3} + P_{2-3-4}\right) + \\ &N_1^2.\frac{di_{3-1}}{dt}\left(P_m + P_3 + P_{2-3} + P_{1-3} + P_{3-4} + P_{1-2-3} + P_{2-3-4} + \right. \\ &\left. P_{1-3-4}\right) + N_1^2.\frac{di_{4-1}}{dt}.\left(P_m + P_{3-4} + P_{2-3-4} + P_{1-3-4}\right) \end{aligned} \tag{18}$$

$$\begin{aligned} v_{4-1} &= N_1^2.\frac{di_1}{dt}\left(P_m + P_{1-4} + P_{1-2-4} + P_{1-3-4}\right) + N_1^2.\frac{di_{2-1}}{dt}\cdot \\ &\left(P_m + P_{2-4} + P_{2-3-4} + P_{1-2-4}\right) + N_1^2.\frac{di_{3-1}}{dt}\cdot \\ &\left(P_m + P_{3-4} + P_{2-3-4} + P_{1-3-4}\right) + N_1^2.\frac{di_{4-1}}{dt}\cdot \\ &\left(P_m + P_4 + P_{1-4} + P_{2-4} + P_{3-4} + P_{2-3-4} + P_{1-2-4} + P_{1-3-4}\right) \end{aligned} \tag{19}$$

D. Definition of Design Parameters

Ferrite 3C94 core has been used with AWG#8 and AWG#16 Litz wire for low voltage and medium voltage windings, respectively. After running a MATLAB optimization code, the following analysis was concluded. In Fig. 4, the variations of B_m, core loss (P_c), winding loss (P_w), sum of core and winding losses (transformer losses, P_{tr}), sum of transformer and switching losses (total losses, P_t), and core and copper weight, have been plotted and demonstrated with respect to A_c and N. Analyzing the graphs shows that for the LV ports, A_c and N being in the range of 34.08-51.12cm^2 and 6-12, respectively, will result in a high transformer efficiency. However, it was noticed that going above 9 turns will increase the core and copper volumes, and in-return, causes an increase in the cost and a reduction in the power density. These results gave a good building block information and starting point for the MV MPSST design phase.

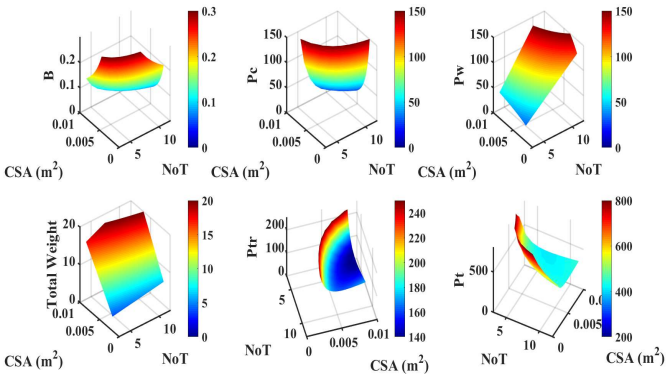

Fig. 4. Results for theoretical calculations.

E. Insulation Requirement

The insulation requirement for a dry-type transformer is explained in IEEE Std. C.57.12.01 and IEEE Std. C57.124. The Basic Impulse Lightning (BIL) test voltage for this MV MPSST transformer shall be in the range of 30kV. The most important limitation regarding the insulation is the effect of the thickness of the insulation materials in the high voltage windings and transformer core. There are two cases here, the first is the need to increase the physical dimensions of the transformer, and the second is that the leakage inductance increases due to the decrease in the coupling coefficient. In-order to ensure proper insulation between windings, 10kV AC polyurethane-nylon (MW80-C) has been used as Litz wires insulation jackets. Moreover, multi-layer Kapton adhesive taped on Nomex818 sheets were inserted as inter-winding insulation layers. These sheets reached more than 32kV of insulation level. In addition, the transformer core must be covered with these insulation sheets in order to avoid insulation breakdown between the core and the medium voltage (MV) terminal cables at 7.4kV potential. Finally, and as a rule of thumb, the LV windings are wrapped first around the transformer mid-leg, and the MV cables at the outer layer to avoid MV/core insulation breakdown.

F. Extracting Four-port Transformer Parameters

Several models have been simulated with different core sizes (34.08-51.12cm^2), number of turns (6-9), and winding arrangements as shown in Fig. 5 and Table 2. Each design is modelled in ANSYS Maxwell-3D, and then co-simulated with a power electronic converter modelled in ANSYS Simplorer. The transformer is tested for different operating conditions with different phase-shift angles. It should be noted that ANSYS just gives the self and mutual inductance matrix between the four ports and does not calculate the leakage and magnetizing inductance values. Therefore, a systematic and theoretical mathematical derivation has been carried out in-order to calculate these inductances values. The MPSST equivalent circuit was derived and the winding arrangements have been taken into consideration in-order to calculate the leakage inductance for all the models of Fig. 5.

As a next step, the four-port transformer is modelled and simulated with ANSYS Maxwell-3D to obtain the inductance matrix. The transformer core is designed with Ferrite MnZn 3C94 core with a number of turns of: $N_{1\text{-}LV} = N_{2\text{-}LV} = N_{3\text{-}LV} = 9$

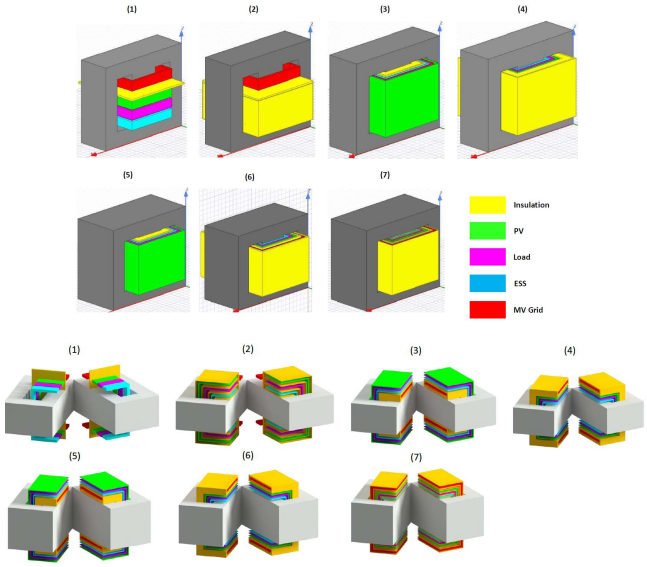

Fig. 5. Investigated MV MPSST design models: Side View & Cut-out.

TABLE Π
DESIGN MODELS DIMENSIONS

Model No.	1	2	3	4	5	6	7
Shapes Used	8U	8U	8U	8U	12U	12U	12U
A_c (cm^2)	34.1	34.1	34.1	34.1	51.1	51.1	51.1
Volume (cm^3)	1122	1122	1122	1122	1683	1683	1683
Efficiency (%)	99.6	99.5	99.0	98.5	99.5	98.5	99.7

turns and $N_{4\text{-MV}}$=130 turns. The inductance matrix for example for model-7 extracted from Maxwell-3D simulation study is given below:

$$\begin{bmatrix} L_{1-1} & M_{1-2} & M_{1-3} & M_{1-4} \\ M_{2-1} & L_{2-2} & M_{2-3} & M_{2-4} \\ M_{3-1} & M_{3-2} & L_{3-3} & M_{3-4} \\ M_{4-1} & M_{4-2} & M_{4-3} & L_{4-4} \end{bmatrix} = \begin{bmatrix} 0.007248 & 0.007245 & 0.007247 & 0.104630 \\ 0.0072459 & 0.007248 & 0.007246 & 0.104661 \\ 0.0072472 & 0.007246 & 0.007248 & 0.104644 \\ 0.104630 & 0.104661 & 0.104644 & 1.512256 \end{bmatrix}$$

The leakage and magnetizing inductances referred to the first winding can be defined as $L_i^1 = N_1^2.P_i$ for i=1,2,3,4; $L_{i-j}^1 = N_1^2.P_{i-j}$ or i=1,2,3 and j=2,3,4 and $i\neq j$, $L_{i-j-k}^1 = N_1^2.P_{i-j-k}$ for i=1,2 and j=2,3 and k=3,4 and $i\neq j\neq k$; and $L_m^1 = N_1^2.P_m$

By substituting the leakage and magnetizing inductance formulas into the induced referred voltage equations (16) - (19) we get:

$$\begin{aligned} \boldsymbol{v}_1 &= \frac{di_1}{dt}\left(L_m^1 + L_1^1 + L_{1-2}^1 + L_{1-3}^1 + L_{1-4}^1 + L_{1-2-3}^1 + L_{1-2-4}^1 + L_{1-3-4}^1\right) + \\ &\frac{di_{2-1}}{dt}.\left(L_m^1 + L_{1-2}^1 + L_{1-2-3}^1 + L_{1-2-4}^1\right) + \\ &\frac{di_{3-1}}{dt}.\left(L_m^1 + L_{1-3}^1 + L_{1-2-3}^1 + L_{1-3-4}^1\right) + \\ &\frac{di_{4-1}}{dt}.\left(L_m^1 + L_{1-4}^1 + L_{1-2-4}^1 + L_{1-3-4}^1\right) \end{aligned} \tag{20}$$

$$\begin{aligned} \boldsymbol{v}_{2-1} &= \frac{di_1}{dt}\left(L_m^1 + L_{1-2}^1 + L_{1-2-3}^1 + L_{1-2-4}^1\right) + \\ &\frac{di_{2-1}}{dt}.\left(L_m^1 + L_2^1 + L_{1-2}^1 + L_{2-3}^1 + L_{2-4}^1 + L_{1-2-3}^1 + L_{2-3-4}^1 + L_{1-2-4}^1\right) + \\ &\frac{di_{3-1}}{dt}.\left(L_m^1 + L_{2-3}^1 + L_{1-2-3}^1 + L_{2-3-4}^1\right) + \\ &\frac{di_{4-1}}{dt}.\left(L_m^1 + L_{2-4}^1 + L_{2-3-4}^1 + L_{1-2-4}^1\right) \end{aligned} \tag{21}$$

$$\begin{aligned} \boldsymbol{v}_{3-1} &= \frac{di_1}{dt}\left(L_m^1 + L_{1-3}^1 + L_{1-2-3}^1 + L_{1-3-4}^1\right) + \\ &\frac{di_{2-1}}{dt}.\left(L_m^1 + L_{2-3}^1 + L_{1-2-3}^1 + L_{2-3-4}^1\right) + \\ &\frac{di_{3-1}}{dt}.\left(L_m^1 + L_3^1 + L_{2-3}^1 + L_{1-3}^1 + L_{3-4}^1 + L_{1-2-3}^1 + L_{2-3-4}^1 + L_{1-3-4}^1\right) + \\ &\frac{di_{4-1}}{dt}.\left(L_m^1 + L_{3-4}^1 + L_{2-3-4}^1 + L_{1-3-4}^1\right) \end{aligned} \tag{22}$$

$$\begin{aligned} \boldsymbol{v}_{4-1} &= \frac{di_1}{dt}\left(L_m^1 + L_{1-4}^1 + L_{1-2-4}^1 + L_{1-3-4}^1\right) + \\ &\frac{di_{2-1}}{dt}.\left(L_m^1 + L_{2-4}^1 + L_{2-3-4}^1 + L_{1-2-4}^1\right) + \\ &\frac{di_{3-1}}{dt}.\left(L_m^1 + L_{3-4}^1 + L_{2-3-4}^1 + L_{1-3-4}^1\right) + \\ &\frac{di_{4-1}}{dt}.\left(L_m^1 + L_4^1 + L_{1-4}^1 + L_{2-4}^1 + L_{3-4}^1 + L_{2-3-4}^1 + L_{1-2-4}^1 + L_{1-3-4}^1\right) \end{aligned} \tag{23}$$

The obtained equivalent circuit the MPSST referred to winding "1" is shown in Fig. 6. Hence, the inductance matrix for the four-winding solid-state transformer will be defined as:

$$\begin{bmatrix} \mathrm{v}_1 \\ \mathrm{v}_2 \\ \mathrm{v}_3 \\ \mathrm{v}_4 \end{bmatrix} = \begin{bmatrix} L_{1-1} & M_{1-2} & M_{1-3} & M_{1-4} \\ M_{2-1} & L_{2-2} & M_{2-3} & M_{2-4} \\ M_{3-1} & M_{3-2} & L_{3-3} & M_{3-4} \\ M_{4-1} & M_{4-2} & M_{4-3} & L_{4-4} \end{bmatrix} . \frac{d}{dt} \begin{bmatrix} \mathrm{i}_1 \\ \mathrm{i}_2 \\ \mathrm{i}_3 \\ \mathrm{i}_4 \end{bmatrix} \tag{24}$$

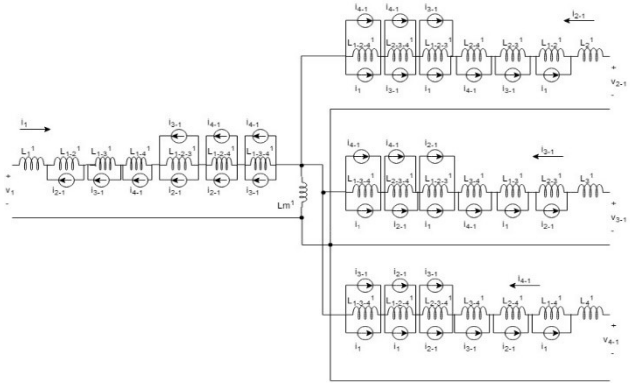

Fig. 6. MPSST equivalent circuit referred to the first port.

Where:

$$\boldsymbol{L}_{1-1} = L_m^1 + L_1^1 + L_{1-2}^1 + L_{1-3}^1 + L_{1-4}^1 + L_{1-2-3}^1 + L_{1-2-4}^1 + L_{1-3-4}^1$$

$$\boldsymbol{L}_{2-2} = \frac{N_2^2}{N_1^2}\left[L_m^1 + L_2^1 + L_{1-2}^1 + L_{2-3}^1 + L_{2-4}^1 + L_{1-2-3}^1 + L_{2-3-4}^1 + L_{1-2-4}^1\right]$$

$$\boldsymbol{L}_{3-3} = \frac{N_3^2}{N_1^2}\left[L_m^1 + L_3^1 + L_{2-3}^1 + L_{1-3}^1 + L_{3-4}^1 + L_{1-2-3}^1 + L_{2-3-4}^1 + L_{1-3-4}^1\right]$$

$$\boldsymbol{L}_{4-4} = \frac{N_4^2}{N_1^2}\left[L_m^1 + L_4^1 + L_{1-4}^1 + L_{2-4}^1 + L_{3-4}^1 + L_{2-3-4}^1 + L_{1-2-4}^1 + L_{1-3-4}^1\right]$$

$$\boldsymbol{M}_{1-2}=\boldsymbol{M}_{2-1}=\frac{N_2}{N_1}\left[L_m^1+L_{1-2}^1+L_{1-2-3}^1+L_{1-2-4}^1\right]$$

$$\boldsymbol{M}_{1-3}=\boldsymbol{M}_{3-1}=\frac{N_3}{N_1}\left[L_m^1+L_{1-3}^1+L_{1-2-3}^1+L_{1-3-4}^1\right]$$

$$\boldsymbol{M}_{1-4}=\boldsymbol{M}_{4-1}=\frac{N_4}{N_1}\left[L_m^1+L_{1-4}^1+L_{1-2-4}^1+L_{1-3-4}^1\right]$$

$$\boldsymbol{M}_{2-3}=\boldsymbol{M}_{3-2}=\frac{N_2.N_3}{N_1^2}\left[L_m^1+L_{2-3}^1+L_{1-2-3}^1+L_{2-3-4}^1\right]$$

$$\boldsymbol{M}_{2-4}=\boldsymbol{M}_{4-2}=\frac{N_2.N_4}{N_1^2}\left[L_m^1+L_{2-4}^1+L_{2-3-4}^1+L_{1-2-4}^1\right]$$

$$\boldsymbol{M}_{3-4}=\boldsymbol{M}_{4-3}=\frac{N_3.N_4}{N_1^2}\left[L_m^1+L_{3-4}^1+L_{2-3-4}^1+L_{1-3-4}^1\right]$$

Based on the specific magnetic structure used in the MV MPSST (Fig. 7), the fluxes present in the core (and hence their corresponding inductances) are: $\phi_m,\phi_1,\phi_2,\phi_3,\phi_4,\phi_{1-2},\phi_{3-4},\phi_{1-2-3},\phi_{2-3-4}$ while $\phi_{1-4}=\phi_{1-3}=\phi_{2-4}=\phi_{2-3}=\phi_{1-2-4}=\phi_{1-3-4}=0$ as they are sandwiched and dictated by the optimized shell-type MPSST winding arrangement. Then, a MATLAB code is developed in order to solve equation (24) in which the leakage and magnetizing inductances are calculated. For instance, for model-7 (μH) we get: $L_m^1=7243.7$, $L_1^1=1.2191$, $L_2^1=-0.0615$, $L_3^1=-0.0386$, $L_4^1=2.2833$, $L_{1-2}^1=1.3571$, $L_{3-4}^1=1.1912$, $L_{1-2-3}^1=2.2587$, $L_{2-3-4}^1=0.961$, $L_{1-4}^1=L_{1-3}^1=L_{2-4}^1=L_{2-3}^1=L_{1-2-4}^1=L_{1-3-4}^1=0$

Based on our derived equivalent circuit given in Fig. 6 and calculated values above, the magnetizing inductance and each ports' leakage inductance value are calculated. For example, for model-7, port-1 leakage inductance $=L_1^1+L_{1-2}^1+L_{1-2-3}^1=1.2191+1.3571+2.2587=4.8349\,\mu H$.

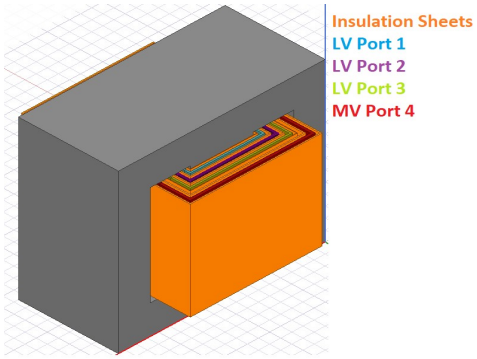

Fig. 7. MV MPSST Maxwell-3D model.

III. Simulation Results

Simulation of the complete system by linking the Maxwell-3D model (physics and magnetics of the transformer) along with Simplorer circuit (power electronics circuit) will result in a complete and realistic simulation of the entire MV MPSST system. After the evaluation of the possible design models for the proposed MV MPPST (Fig. 5), Maxwell-3D/ Simplorer co-simulation studies are carried out (Fig. 8). The ports voltages of the system are 7.4kVDC for MV grid port and 500VDC for energy storage, PV, and load ports. The simulation is carried out at 50kHz switching frequency and at full load to deliver 25kW to the load port. The duty cycle of the PWM signals are kept constant at 50% and power control is obtained by controlling the phase-shift angles among the H-bridge converters. The obtained results from the simulation studies are compared in terms of core shape, effective cross-sectional area, volume, transformer losses, and efficiency. Comparison showed that the leakage inductance is adversely affected in terms of the insulation and placement of the high voltage winding. As a result, besides the parameters such as size and efficiency, lower leakage inductance has been chosen as the main target. Results showed that model-7 provides the lowest leakage inductance with the highest efficiency level. The flux distribution of this model is given in Fig. 9. It is seen that the maximum flux density is around 0.11691T which is below the design target limit that is defined by ferrite material specifications. The detailed parameters of the selected optimal model are given in Table 3. As seen from the results, the total loss of the transformer is obtained as 73.4W, and then the efficiency of the transformer is calculated as 99.7%.

Fig. 10 shows the ports currents and voltages waveforms obtained from ANSYS Maxwell-3D/ANSYS-Simplorer co-simulation results for Model-7. As can be seen from the figure, while the PV and grid port currents are in one direction, the load and energy storage port currents are in reverse direction. At this instant, the grid and PV ports are delivering power to the load and energy storage ports. Besides, the losses of the transformer and efficiency of the proposed transformer is calculated and variation of the transformer efficiency versus load level is given in Fig. 10(c).

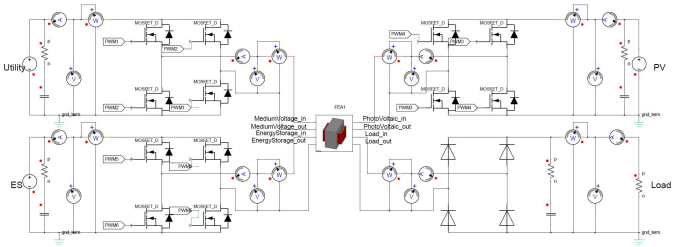

Fig. 8: Maxwell-3D/Simplorer Transient-Transient Co-Simulation model

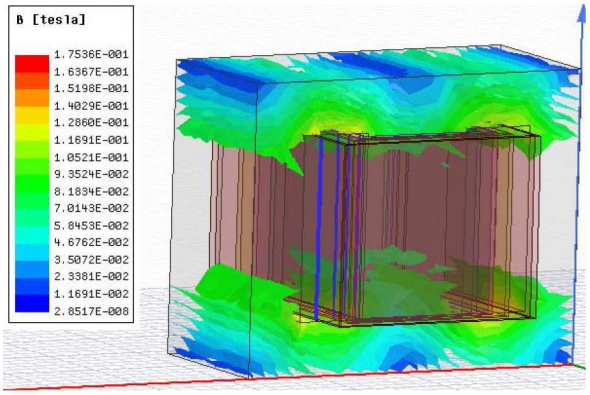

Fig. 9. Model-7 Flux Distribution.

TABLE III
OPTIMAL DESIGN PARAMETERS

Parameter		Value
No. of Turns		9/9/9/130
Litz Wire (AWG)		2x8/2x8/2x8/16
B_{max} (T)		0.11691
Leakage Ind. (µH)	ES	4.834
	Load	4.515
	Grid	925.431
	PV	4.372
Magnetizing Inductance (µH)		7243.7
Transformer Losses (W)		73.4
Efficiency (%)		99.7
Effective Area (cm^2)		51.120
Core Volume (cm^3)		1683

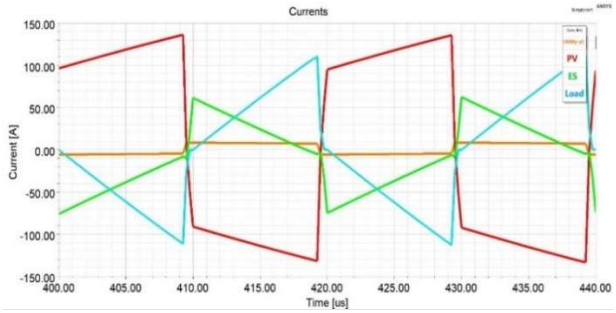

(a) Waveforms of port currents

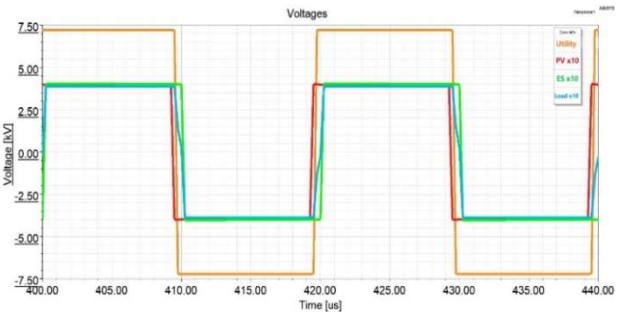

(b) Waveforms of port voltages

(c) Efficiency versus load level variation of the proposed transformer

Fig. 10. Simulation results for Model-7.

IV. EXPERIMENTAL SETUP AND TEST RESULTS

After the desired design specifications are achieved for simulation studies, the designed transformer is built. In Fig. 11a, a picture of the built transformer is shown. The windings are placed on the middle leg core with interwinding insulation layers. All three low voltage port windings are wrapped together to increase the coupling coefficient. Core to core, winding to winding, and core to winding insulation are carefully considered in this process. A cold plate is used for thermal management and heat dissipation. As a final process, the transformer can be potted to improve both the insulation and the thermal conductivity. However, since this structure was used in experimental studies, this method was not used.

To test the transformer, three DAB converters are designed and implemented using 1.2kV SiC MOSFETs. Since the MV port is considered as the load port (for testing purposes as high voltage switches are not available), a MV bridge rectifier is implemented by using SiC Diodes with 1.7kV voltage rating. Six series-connected diodes were used for each MV bridge rectifier's single diode at the load side and complete rectifier unit is given in Fig. 11b. MV load port is loaded with 13.6kOhm resistor bank and an external 20uH to limit the peak current at the LV switches side. The experimental set-up implemented to test the designed MV four-port MPSST is depicted in Fig. 12. All MOSFET modules and drivers, control board, signal conditioning board, MV four-port transformer, and MV rectifier can be seen from the figure.

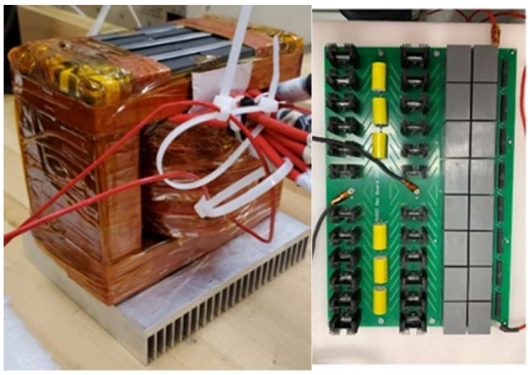

(a) (b)

Fig. 11. (a) The designed transformer (186/152/90mm Width/Height/Depth). (b) MV Bridge Rectifier at the load side.

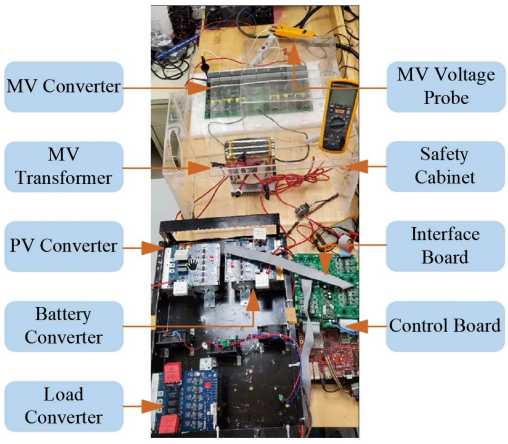

Fig. 12. MV four-port transformer test set-up.

For limitation in switches current and power supply used, two ports were tested to reach and validate the 7.4kV at 4kW power level. To test the system, voltage level was increased gradually. In Figs. 13 and 14, waveforms of the port voltages

and currents are depicted for 3.6kV and 5.6kV, respectively. Then, the system is tested at its rated value 7.4kV as can be seen in Fig. 15. As it can be seen from the figures there is a low frequency swinging. Since availability of the high voltage switches are limited, in this study, (as explained above) serial connected 1.7kV diodes are used to design the rectifier used in the MV port. Similar situation is valid for the DC capacitors, serial connected capacitors are used to reach up to 7.4kV. In addition, for safety reasons, long Litz wires are used to connect the transformer to the MV bridge rectifier PCB. However, the resultant inductances of the connection port and parasitic capacitances of the rectifier interact and cause the swinging seen in the testing result waveforms. In these figures, the MV voltage probe attenuation factor is 2000 while the maximum factor in the oscilloscope is 1000 (Model CT4079). Therefore, the real MV port voltage is twice the voltage measured by the oscilloscope. As the medium voltage has been verified, the next step will be to lower the voltage (again, power supply limitation) and test all the ports and analyze the power flow with the closed loop control implemented [21].

When the experimental and simulation results are compared, it is seen that the results are consistent. Thus, the four-port converter structure capable of 50kHz switching has been successfully tested at 7.4kV medium voltage level.

Fig. 13. Primary Voltage (Probe 3) and Current (Probe 2), and Medium Voltage 3.6kV (Port 1)

Fig. 14. Primary Voltage (Probe 3) and Current (Probe 2), and Medium Voltage 5.6kV (Port 1)

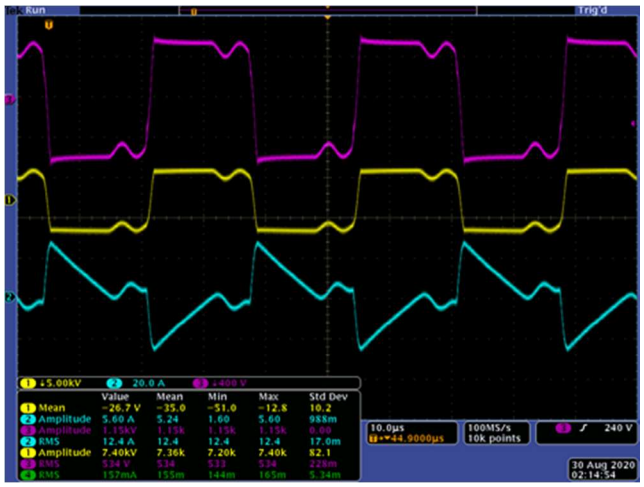

Fig. 15. Primary Voltage (Probe 3) and Current (Probe 2), and Medium Voltage 7.4kV (Port 1)

V. Conclusion

In this study, a four-port SST which can connect four different load or source ports together is designed for microgrid applications. One port of the transformer is designed to be operate at MV (compatible with 4.16kV AC voltage). Different design models are considered, and optimal design is obtained. The obtained design model simulated and with FEA software and 99.7% transformer efficiency is obtained. Then, the designed transformer is implemented. In addition, to test the transformer, a test set-up including LV full-bridge converters, MV rectifier is implemented. 7.4kV voltage level is reached and validated.

References

[1] W. Shen, F. Wang, D. Boroyevich and C. W. Tipton, "Loss Characterization and Calculation of Nanocrystalline Cores for High-Frequency Magnetics Applications," *IEEE Transactions on Power Electronics*, vol. 23, no. 1, pp. 475-484, Jan. 2008.

[2] W. A. Reass *et al*., "High-frequency multimegawatt polyphase resonant power conditioning," *IEEE Transactions on Plasma Science*, vol. 33, no. 4, pp. 1210-1219, Aug. 2005.

[3] M. K. Das *et al*., "10 kV, 120 A SiC half H-bridge power MOSFET modules suitable for high frequency, medium voltage applications," *IEEE Energy Conv. Congress and Expo.*, Phoenix, AZ, 2011, pp. 2689-2692.

[4] A. E. Shafei, S. Ozdemir, N. Altin, G. Jean-Pierre and A. Nasiri, "A High Power High Frequency Transformer Design for Solid State Transformer Applications," *2019 8th International Conference on Renewable Energy Research and Applications (ICRERA)*, Brasov, Romania, 2019, pp. 904-909, doi: 10.1109/ICRERA47325.2019.8996515.

[5] G. Jean-Pierre, M. Khayamy, N. Altin, A. E. Shafei and A. Nasiri, "A Triple Phase-Shift Based Control Method for RMS Current Minimization and Power Sharing Control of Input-Series Output-Parallel Dual Active Bridge Converter," *2020 IEEE Transportation Electrification Conference & Expo (ITEC)*, Chicago, IL, USA, 2020, pp. 550-555, doi: 10.1109/ITEC48692.2020.9161578.

[6] S. Balci, I. Sefa, and N. Altin, "Design and analysis of a 35 kVA medium frequency power transformer with the nanocrystalline core material", *International Journal of Hydrogen Energy*, vol.42, no.28, pp.17895-17909, 2017.

[7] S. Roy, A. De and S. Bhattacharya, "Current source inverter based cascaded solid-state transformer for AC to DC power conversion," *2014 International Power Electronics Conference (IPEC-Hiroshima 2014 - ECCE ASIA)*, Hiroshima, 2014, pp. 651-655.

[8] H. Fan and H. Li, "High-Frequency transformer isolated bidirectional dc–dc converter modules with high efficiency over wide load range for 20 kVA Solid-State Transformer," *IEEE Transactions on Power Electronics*,

vol. 26, no. 12, pp. 3599-3608, Dec. 2011.

[9] T. Zhao, L. Yang, J. Wang and A. Q. Huang, "270 kVA Solid State Transformer Based on 10 kV SiC Power Devices,"*2007 IEEE Electric Ship Technologies Symposium*, Arlington, VA, 2007, pp. 145-149.

[10] Hengsi Qin and J. W. Kimball, "Ac-ac dual active bridge converter for solid state transformer," *2009 IEEE Energy Conversion Congress and Exposition*, San Jose, CA, 2009, pp. 3039-3044.

[11] S. Ozdemir, S. Balci, N. Altin and I. Sefa, "Design and performance analysis of the three-level isolated DC-DC converter with the nanocyrstalline core transformer", *International Journal of Hydrogen Energy*, vol.42, no.28, pp.17801-17812, 2017.

[12] A. C. Nair and B. G. Fernandes, "A novel multi-port solid state transformer enabled isolated hybrid microgrid architecture,"*43rd Annual Conf. of the IEEE Ind. Electronics Society*, Beijing, 2017, pp. 651-656.

[13] M. Rashidi, A. Bani-Ahmed, and A. Nasiri, "Application of a multi-port solid state transformer for volt-VAR control in distribution systems," *IEEE Power&Energy Society General Meeting*, Chicago, IL, 2017, pp.1-4.

[14] M. Rashidi, A. Bani-Ahmed, R. Nasiri, A. Mazaheri and A. Nasiri, "Design and implementation of a multi winding high frequency transformer for MPSST application," *IEEE 6th Int. Conf. on Renewable Energy Research and Applications*, San Diego, CA, 2017, pp. 491-494.

[15] V. N. S. R. Jakka and A. Shukla, "A triple port active bridge converter based multi-fed power electronic transformer, "*2016 IEEE Energy Conv. Congress and Exposition (ECCE)*, Milwaukee, WI, 2016, pp. 1-8.

[16] W. L. Malan, D. M. Vilathgamuwa, G. R. Walker and M. Hiller, "A three port resonant solid state transformer with minimized circulating reactive currents in the high frequency link,"*2016 IEEE 2nd Annual Southern Power Electronics Conference (SPEC)*, Auckland, 2016, pp. 1-6.

[17] A. El Shafei, S. Ozdemir, N. Altin, G. Jean-Pierre and A. Nasiri, "A Complete Design of a High Frequency Medium Voltage Multi-Port Transformer," *2019 8th International Conference on Renewable Energy Research and Applications (ICRERA)*, Brasov, Romania, 2019, pp. 761-766, doi: 10.1109/ICRERA47325.2019.8997088.

[18] G. Jean-Pierre, A. El Shafei, N. Altin and A. Nasiri, "A Multiport Bidirectional LLC Resonant Converter for Grid-Tied Photovoltaic-Battery Hybrid System," *2019 8th International Conference on Renewable Energy Research and Applications (ICRERA)*, Brasov, Romania, 2019, pp. 755-760, doi: 10.1109/ICRERA47325.2019.8996775.

[19] A. El Shafei, S. Ozdemir, N. Altin, G. Jean-Pierre and A. Nasiri, "Design and Implementation of a Medium Voltage, High Power, High Frequency Four-Port Transformer," *2020 IEEE Applied Power Electronics Conference and Exposition (APEC)*, New Orleans, LA, USA, 2020, pp. 2352-2357, doi: 10.1109/APEC39645.2020.9124337.

[20] Tong, Anping, Lijun Hang, Guojie Li, Xiuchen Jiang, and Shenyu Gao. "Modeling and analysis of a dual-active-bridge-isolated bidirectional DC/DC converter to minimize RMS current with whole operating range." IEEE Transactions on Power Electronics 33, no. 6 (2017): 5302-5316.

[21] S. Ozdemir, N. Altin, A. E. Shafei, M. Rashidi and A. Nasiri, "A Decoupled Control Scheme of Four-Port Solid State Transformer," *2019 IEEE Energy Conversion Congress and Exposition (ECCE)*, Baltimore, MD, USA, 2019, pp. 5009-5015, doi: 10.1109/ECCE.2019.8912595.

[22] Qing Chen, F. C. Lee, Jian Zhong Jiang and M. M. Jovanovic, "A new model for multiple-winding transformer," *Proceedings of 1994 Power Electronics Specialist Conference - PESC'94*, Taipei, Taiwan, 1994, pp. 864-871 vol.2.

[23] *Hsu, Shi-Ping (1980)* Problems in analysis and design of switching regulators: I. Pole placement technique for DC-to-DC switching regulators. II. Transformer modelling. III. Cross-regulation of the two-output Cuk converter. *Dissertation (Ph.D.), California Institute of Technology. http://resolver.caltech.edu/CaltechETD:etd-10302006-100214.*

Ahmad El Shafei (M'09) received his B.E in Electrical & Computer Engineering (Honors) from American University of Beirut, Lebanon in 2013. He worked as a power system engineer in oil & gas field until 2016. He is currently pursuing his PhD in Electrical Engineering from University of Wisconsin Milwaukee. His research is on power electronics design focusing on high power, medium voltage, high frequency transformer design, build, and testing. He worked at Eaton Research Lab and Imagen Energy, both based in Milwaukee, WI. He is an IEEE member since 2009 and received Best Paper Award from 8th International Conference on Renewable Energy Research and Applications (ICRERA 2019).

Saban Ozdemir (S'12-M'14-SM'19) received the B.Sc., M.Sc., and Ph.D. degrees in electrical education from Gazi University, Ankara, Turkey, in 2004, 2007m and 2013, respectively. From 2008 to 2009, he was with Baskent University, Ankara, Turkey. In 2009, he joined Gazi University. He is currently an Associate Professor with the Department of Electrical and Electronics Engineering, Faculty of Technology, Gazi University. From 2017 to 2018, he was a Visiting Scholar and from 2018 to 2019, he was a Research Associate with the University of Wisconsin-Milwaukee, Milwaukee, WI, USA. His current research interests include power electronics, uninterruptible power supplies, grid interactive inverters, solid-state transformers, and resonant converter. He is currently an Associate Editor for the IEEE Transactions on Industry Applications for Renewable and Sustainable Energy Conversion Systems Committee.

Necmi Altin (M'11-SM'19) received the B.Sc., M.Sc. and Ph.D. degrees from Gazi University, Ankara, Turkey, in 2000, 2003, and 2009, respectively. He joined to the Department of Electrical and Electronics Engineering, Faculty of Technology, Gazi University as an Assistant Professor in 2010, and he was promoted to Associate Professor and Full Professor positions in 2014 and 2020, respectively. He has been a Visiting Scholar at University of Wisconsin-Milwaukee, USA from 2017 to 2019. His current research interests include power electronics, application of power electronics in renewable energy systems, high power factor rectifiers, grid interactive inverters, solid state transformers, and control systems. He has authored and co-authored over 150 journal and conference papers, and a book chapter. Dr. Altin is currently serving as the Associate Editor of the IEEE Transactions on Industry Applications for Renewable and Sustainable Energy Conversion Systems Committee. He received Best Paper Award from 8th International Conference on Renewable Energy Research and Applications (ICRERA2019) and 13th International Conference on Electronics, Computers and Artificial Intelligence (ECAI2021).

Garry Jean-Pierre received his B.S., M.S., and PhD degrees in electrical engineering from the University of Wisconsin - Milwaukee in 2016, 2017, and 2021, respectively. He is currently a Lead Embedded Systems Engineer for Eaton Corporation at the Eaton Research Lab in Menomonee Falls, Wisconsin. His research interests include power electronics, renewable energy systems, microgrids, and embedded controller design. He is a former research and teaching assistant for the College of Engineering and Applied Sciences at the University of Wisconsin - Milwaukee.

Adel Nasiri received B.S. and M.S. degrees from Sharif University of Technology, Tehran, Iran, in 1996 and 1998, respectively, and the PhD degree from Illinois Institute of Technology, Chicago, Illinois, in 2004, all in electrical engineering.

He is presently a Distinguished Professor in the Electrical Engineering Department at the University of South Carolina. His research interests are smart and connected energy systems, energy storage, and microgrids. Previously, he worked at the University of Wisconsin-Milwaukee (UWM) from 2005 to 2021 and served in various roles including professor of electrical engineering, founding and Interim Executive Director, Connected Systems Institute (CSI) and Director, Center for Sustainable Electrical Energy, and the site director for the NSF center on Grid-connected Advanced Power Electronic Systems (GRAPES). He has published numerous technical journal and conference papers and co-authored two books on related topics. He also holds seven patent disclosures.

Dr. Nasiri is currently the chair of IEEE Industry Applications Society (IAS) Committee on renewable and sustainable energy conversion. He is also an Editor of Power Components and Systems, and Associate Editor of the International Journal of Power Electronics and was an Editor of IEEE Transactions on Smart Grid (2013-2019) and paper review chair for IAS (2018-2019). He was the general Chair of 2012 IEEE Symposium on Sensorless Electric Drives, 2014 International Conference on Renewable Energy Research and Applications (ICRERA 2014), and 2014 IEEE Power Electronics and Machines for Wind and Water Applications (PEMWA 2014).